Comparison between Cassini and Voyager observations of Jupiter's decametric and hectometric radio emissions

Masafumi Imai,[1,2] Kazumasa Imai,[3] Charles A. Higgins,[4] and James R. Thieman[5]

Received 7 January 2011; revised 14 October 2011; accepted 17 October 2011; published 30 December 2011.

[1] In this paper, we attempt to clarify the relationship between Jovian hectometric (HOM) and non-Io-related decametric (non-Io-DAM) radio structure. For that purpose, we extend the analysis by including more data and investigating statistical properties of the Jovian DAM and HOM radio emissions based on Cassini and Voyager observations, especially below 16 MHz. We have investigated these emissions observed by the Cassini, Voyager 1, and Voyager 2 spacecraft for specific Jovigraphic latitudes in the range of −3.7°–7.3° and local times in the range of 0.76–21.4 hours. We show a statistical comparison of Cassini, Voyager 1, and Voyager 2 data for occurrence probability in Central Meridian Longitude (CML) versus Io phase and in CML versus Frequency. The main results are as follows: (1) the detailed frequency structures of non-Io-related components can be seen for different spacecraft's local time and Jovigraphic latitude, (2) the high frequency of HOM extends up to near 10 MHz, and (3) a new DAM component, named the non-Io-D, appears from 40° to 60° CML in the frequency range of 7–11 MHz. On the basis of additional information of different behaviors of non-Io-B and non-Io-A structures in longitude depending on pre- and post-encounter of Cassini data, we improved the DAM angular beaming model that shows the cone half-angle of the emitting cone decreases as a function of frequency. We conclude that the changing beaming angle is not affected by Jovigraphic latitude of the spacecraft, but rather due to different local time of the source regions.

Citation: Imai, M., K. Imai, C. A. Higgins, and J. R. Thieman (2011), Comparison between Cassini and Voyager observations of Jupiter's decametric and hectometric radio emissions, *J. Geophys. Res.*, *116*, A12233, doi:10.1029/2011JA016456.

1. Introduction

[2] Thousands of hours of ground-based radio telescope observations in the decametric radio wavelengths (DAM) have determined that observed radio emission probability is correlated with the Central Meridian Longitude (CML) of Jupiter. Three main CML regions where the probability of detection is greatest have been identified and designated as sources A, B, and C [*Carr et al.*, 1961]. *Bigg* [1964] discovered that the probability of detection of emission from the three major sources is strongly affected by the position of Io with respect to superior geocentric conjunction; this angle is known as "Io Phase".

[3] The first observations of Jupiter's hectometric (HOM) radio emissions below the ionospheric critical frequency were made by *Desch and Carr* [1974] using data from the RAE-1 satellite and by *Brown* [1974] using IMP-6 data. Most of our initial knowledge of the HOM emission came from the observations by the Planetary Radio Astronomy (PRA) instrument on-board Voyager 1 and 2 spacecraft [*Warwick et al.*, 1979a, 1979b].

[4] Jupiter's DAM and HOM radio emissions originate from interactions between the magnetospheric plasma and the strong magnetic field of Jupiter. They are still not clearly understood due to their complex phenomenology and limited observation conditions [see *Carr and Desch*, 1976; *Carr et al.*, 1983; *Ladreiter and Leblanc*, 1991; *Zarka*, 1998; *Clarke et al.*, 2004, and references therein]. Because the Jovian DAM and HOM emission frequency ranges are right next to each other, the relationship between them is very important to help understand the emission scenario. In this paper, we will focus on this issue.

[5] Since the terrestrial ionosphere limits the ground-based reception of radio waves to approximately 15 MHz and above, only the higher frequency emissions can be usefully studied from the Earth. By contrast, the observable frequency range on spacecraft is limited by on-board receiver capability and solar wind plasma frequency. So far, only the PRA instrument aboard Voyager was designed to fully record Jupiter's DAM and HOM emissions. Yet it was very difficult to follow the maxima and minima of the intensity distribution in the time–frequency plot as frequency varied from 15 MHz down to 5 MHz. This was due to spacecraft-generated interference concealing observations below 10 MHz in the high

[1]Advanced Course in Mechanical and Electrical Engineering, Kochi National College of Technology, Kochi, Japan.
[2]Now at Department of Geophysics, Kyoto University, Kyoto, Japan.
[3]Department of Electrical Engineering and Information Science, Kochi National College of Technology, Nankoku, Japan.
[4]Department of Physics and Astronomy, Middle Tennessee State University, Murfreesboro, Tennessee, USA.
[5]Solar System Exploration Division, NASA Goddard Space Flight Center, Greenbelt, Maryland, USA.

Copyright 2011 by the American Geophysical Union.
0148-0227/11/2011JA016456

frequency receiver, and due to the variation of sensitivity and frequency coverage between high and low frequency receivers.

[6] Jupiter's moon Io plays an important role in the generation of Jupiter's DAM emissions, such that the emissions are usually classified as Io-related (Io-DAM) and non-Io-related (non-Io-DAM) emissions. In contrast to DAM, HOM is not controlled by Io [*Higgins et al.*, 1998; *Zarka et al.*, 2001]. The higher frequencies of Io-DAM and non-Io-DAM are believed to extend up to the cutoff frequencies of 39.5 MHz and 38 MHz, respectively [*Carr et al.*, 1983], whereas the lower frequencies are both a few MHz. The lower frequency of HOM is usually observed down to 300 kHz, and 40 kHz at a minimum, while the higher frequency of HOM is inferred to be 3 MHz (i.e., upper limit of the definition of the term "HOM") [*Carr et al.*, 1983] and 7 MHz [*Barrow and Desch*, 1989].

[7] It is well known that the link between non-Io-DAM and HOM is not clearly understood, since the frequencies between 3 MHz and 10 MHz have been difficult to study. Some of these have been reviewed by *Ladreiter and Leblanc* [1991]. There is evidence that non-Io-DAM is a higher frequency part of HOM, since (1) a better correlation between HOM and non-Io-DAM emissions has been found [*Genova et al.*, 1987], (2) solar wind control was presented for both HOM and non-Io-DAM [e.g., *Terasawa et al.*, 1978; *Barrow and Desch*, 1989], (3) a local time effect has been shown for non-Io-DAM and HOM [*Alexander et al.*, 1981; *Leblanc*, 1981; *Barrow*, 1981a; *Menietti et al.*, 1999], and (4) it is found that a positive correlation exists between the radio intensity of non-Io-DAM and HOM and the intensity of UV auroras [*Prangé et al.*, 1993; *Gurnett et al.*, 2002]. The local time effect is dependent on the observing position of the spacecraft relative to the local time positions on Jupiter determined by the Sun, with noon being the longitudinal meridian pointed toward the Sun. There is an observed local time dependence for the sources, but because the emission from the sources is believed to be in the form of hollow cones the actual longitude of the emission sources is not at the same longitude as the observer, but at higher or lower longitudes and therefore also at a different local time than the observer.

[8] It is widely believed that Jupiter's DAM and HOM emissions are generated in the right-hand extraordinary (R-X) mode via the cyclotron maser instability (CMI) [*Wu and Lee*, 1979]. The HOM source has been considered to be along Jovian magnetic field lines with the L-shell ≥ 7 and ≤ 11 [*Ladreiter et al.*, 1994] or L-shell ≥ 10 [*Menietti et al.*, 2003] (i.e., a dipolar magnetic field line from the planet's center intersects the equatorial plane at a distance of 7 to 11 planetary radii or of 10 planetary radii or greater, respectively). Io-DAM is mostly accepted to originate along the magnetic field line with the L-shell parameter ≈ 5.9, belonging to the flux tube passing through Io [e.g., *Imai et al.*, 1997, 2002; *Queinnec and Zarka*, 1998; *Ray and Hess*, 2008]. In contrast with Io-DAM, the L-shell value of the sources of the non-Io-DAM has been thought to extend along L-shell ≥ 7 field lines [see *Zarka*, 1998; *Clarke et al.*, 2004, and references therein]. But measurement by the modulation lane method shows the source L-shell value is close to 5.9 inside the Io plasma torus region [*Imai et al.*, 2002].

[9] The maximum of the average intensity of DAM and HOM was found by *Zarka et al.* [2004] using Jupiter's radio emissions detected by the Cassini Radio and Plasma Wave Science (RPWS) instrument. They state that the peak of the average intensity of DAM and HOM is at 1–2 MHz and the trend of the average intensity gradually decreases up to 10 MHz and then decreases further.

[10] In a statistical study of Jovian DAM and HOM radiation, *Menietti et al.* [1999] compared combined Galileo observations from 3.2 to 5.6 MHz with the combined ground observations at 18, 20, and 22 MHz based on occurrence probability as a function of CML of System III. As a result, they found slightly different trends of the CML occurrence probability histograms between Galileo and ground observations. The reasons for the differences are that the frequencies studied are lower, the position of each source is related to the magnitude of magnetic field (i.e., as frequency decreases, the position of the source gradually moves as the field line curves away from the surface of Jupiter), and because the wave normal angle is inferred to depend on frequency. Therefore they concluded that the frequencies from 3.2 to 5.6 MHz by Galileo spacecraft are a lower part of DAM. However, *Barrow and Desch* [1989] used a similar method and analyzed frequencies at 5–7, 10, 18 MHz by ground stations, and 1307 kHz by Voyager 2. They found that one of HOM peaks at about 20° CML can be seen from the 1307 kHz to the 5–7 MHz profiles and to a low peak in the 10 MHz profile. They concluded that the peak near 20° CML is a part of HOM which extends up to the frequency at 5–7 MHz. It is important to note that previous studies show that there are still gaps in frequency coverage between 5.6 MHz and 18 MHz [*Menietti et al.*, 1999] and between 5–7 MHz and 10 MHz [*Barrow and Desch*, 1989].

[11] Recently, *Imai et al.* [2008], using all the data during Cassini flyby, first recognized the "V-shape" pattern within non-Io-DAM, which was originally suggested by *Thieman and Smith* [1978] and *Alexander et al.* [1981], in the frequency versus longitude plot between 9 MHz and 16 MHz. Moreover, there are two enhanced peaks at 160° and 240° CML at 16 MHz. As frequency decreases toward 9 MHz, only one peak occurs near 205° CML. The peak gradually disappeared below 9 MHz.

[12] In this paper, we will extend the analysis on the HOM/DAM structure by including more data and investigating statistical properties of the Jovian DAM and HOM radio emissions based on Cassini and Voyager observations, especially below 16 MHz. In section 2, we briefly describe the radio receiver and antenna system of Cassini and Voyager. We state the rotation based averaging method is applicable to identification of the observations of Jovian DAM and HOM within interference in section 3.1. Moreover, we report on the statistical result of Jupiter's DAM and HOM in CML versus Io phase diagrams as well as CML versus frequency in terms of non-Io-DAM and HOM in sections 3.2 and 3.3, respectively. In section 4 we incorporate new data and report an improved beaming model based on the angular beaming model of *Imai et al.* [2008] as well as the locations of non-Io-DAM.

2. Data and Observations

[13] Although Jupiter's DAM and HOM radio emissions can be observed from ground-based observations (e.g., Nançay Decameter Array in France [*Boischot et al.*, 1980;

Table 1. Cassini and Voyager Spacecraft Data Collection Summary

Spacecraft	Observations Used in This Study	Spacecraft Jovigraphic Latitude	Local Time Coverage	Rotations of Jupiter
Cassini	2-Oct-00 – 21-Mar-01	+3.7° – −3.7°	10.6–21.4 hours	339
Voyager 1	6-Feb-79 – 7-Apr-79	+3.2° – +5.3°	10.4–4.4 hours	133
Voyager 2	8-Jun-79 – 30-Jul-79	+7.3° – +5.2°	9.5–3.0 hours	122

Lecacheux, 2000]) and spacecraft around Earth (e.g., Wind/WAVES [*Bougeret et al.*, 1995]), the data obtained by the Cassini, Voyager 1, and Voyager 2 spacecraft have higher signal-to-noise ratio at DAM frequencies with much less interference and a wide geometrical coverage. In particular we are interested in frequencies between 5 MHz and 16 MHz corresponding to the lower spectral region of DAM and the upper spectral region of HOM emission. Moreover, for frequencies below 16 MHz, data from these spacecraft can be compared with each other.

[14] The Cassini spacecraft was equipped with the RPWS instrument having five on-board receivers that monitored the electric fields from 1 Hz to 16 MHz. The high frequency receiver (HFR) covers the frequency range from 3.5 kHz to 16 MHz and consists of two sets of four analog receivers with a digital signal processing unit. It is connected to three 10 m long monopole electric field antennas, called here E_U, E_V, and E_W. These are used to receive electric field signals. The E_U and E_V monopoles are configured at an angle of 120° and both are nearly orthogonal to the E_W monopole. For a full description of the RPWS instrument see *Gurnett et al.* [2004]. Only the upper bands of HFR (HF1 and HF2) were used for the present study and were operated for Jupiter's encounter only. HF1 and HF2 had a sweep period of 32 s over 76 frequency channels, between 0.325 MHz and 4.075 MHz in 50 kHz steps, and 61 channels, from 4.025 to 16.025 MHz every 200 kHz, respectively.

[15] The PRA instrument on the Voyager spacecraft was composed of two on-board receivers that recorded the electric fields at center frequencies ranging from 1.2 kHz to 40.2 MHz. The high band receiver is connected to two orthogonal electric antennas, each of length 10 m, and covers the frequency range from 1.3 to 40.2 MHz. It sweeps through 128 channels every 6 s, but the 48-second time-averaged data, provided by Voyager PRA team, is used here. For a detailed description of the PRA instrument see *Lang and Peltzer* [1977] and *Warwick et al.* [1977, 1979a, 1979b].

[16] In order to directly compare the variation of Jupiter's DAM and HOM emissions depending upon Jovigraphic latitude, we have analyzed the data observed by Cassini, Voyager 1, and Voyager 2. The general geometric parameters used in this study are given in Table 1 and also summarized in Figure 1. Note that, because the geometrical parameters of the spacecraft were rapidly changing near Jupiter's closest approach, we have neglected the data when the Voyager 1 and 2 spacecraft and the Cassini spacecraft were inside of 25 R_J and 200 R_J, respectively.

3. Occurrence Probability

[17] To analyze the nature of Jupiter's radio emissions, it is best to make a map of Jupiter's radio occurrence probability plotted as a function of CML of System III [*Higgins et al.*, 1996] and Io phase. This map plays a role in easily understanding the influence of Io-related and non-Io-related emissions and pointing out the regions where the occurrence probability is relatively high as a statistical point of view.

[18] Although the catalogs of Jupiter's DAM emissions observed by Voyager 1 and Voyager 2 during Jupiter's flyby have already been published by *Barrow* [1981b] and *Aubier and Genova* [1985], they did not sort the occurrence probability plots by each frequency (i.e., an individual channel of PRA receiver). Since Jupiter's DAM radio emissions have the features of arclike shapes that curve like opening and closing parentheses, called vertex early arcs (VEA) and vertex late arcs (VLA) on the time–frequency plot [*Warwick et al.*, 1979a], the individual frequency profile plays a role in investigating their phenomenology. In addition, depending upon the upper frequency limit of these emissions, they are classified into two arcs: the greater arc, from a few MHz to 30–40 MHz, and the lesser arc, from a few MHz to 20 MHz [*Boischot et al.*, 1981]. Furthermore, *Barrow* [1981b] and *Aubier and Genova* [1985] did not investigate the occurrence probability at the frequencies below 15 MHz, due in part to interference from the instruments on-board Voyager. Therefore, we focus on the analysis of the occurrence probability for each frequency

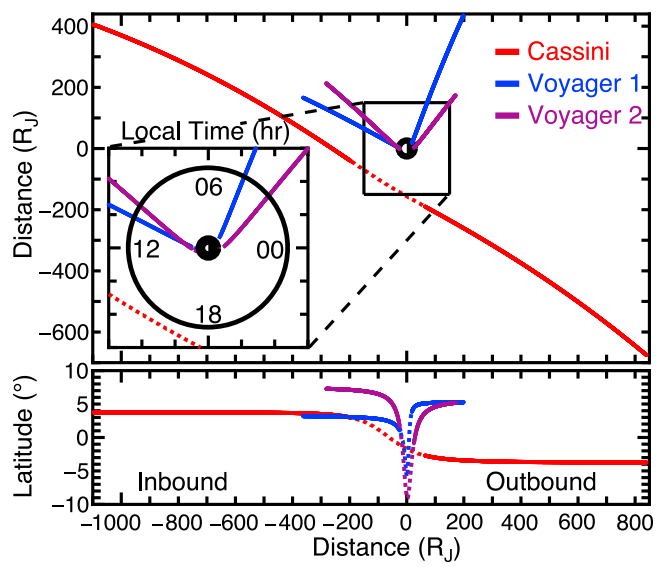

Figure 1. This graph shows the Cassini, Voyager 1, and Voyager 2 trajectories. The upper plot shows the local time coverage of each spacecraft and the view from the north pole of Jupiter. The lower plot shows the Jovigraphic latitude from the equatorial plane. These segments of the trajectory are plotted in the opposite of Jupiter Solar Equatorial (JSE) coordinate system. The solid lines indicate the data used in this study. Since the geometry of Cassini and Voyager 1 and 2 rapidly changed during the closest approach to Jupiter, the data are neglected within 200R_J in Cassini spacecraft, and within 25R_J in Voyager 1 and 2 spacecraft, as shown by the dashed lines.

based on Voyager 1 and Voyager 2 as well as Cassini observations.

3.1. Analysis Method

[19] In this section we review our analysis technique, called rotation based averaging method, in detail. It is important to note that this technique is a powerful tool for analysis since it removes any local time effects and long-term changes in data reception, and minimizes the quasi-random background fluctuation affected by the interference of the spacecraft itself. This technique has already been performed by *Higgins et al.* [2006], *Higgins* [2007], and *Imai et al.* [2008].

[20] First, all the data from Cassini and Voyager are calibrated and normalized to the intensity corresponding to 100 R_J distance for each frequency channel. The data are organized by Jupiter's rotation. Second, we deduce the mean intensity (μ) and standard deviation (σ) for each rotation of Jupiter. In this study, we define the independent threshold, the mean intensity plus one fifth standard deviation (μ + 0.2 σ) for the Cassini case and the mean intensity plus one standard deviation (μ + 1 σ) for the Voyager case, since the receiver sensitivity is different compared with Voyager/PRA and Cassini/RPWS [*Zarka and Kurth*, 2005]. Figure 2a, for example, shows the variation of calibrated intensity obtained by the Cassini data at the E_U antenna at 16.025 MHz as small dots based on Jovian CML. The blue and red lines indicate the mean intensity and the rotation-threshold, defined as μ + 0.2 σ, respectively in the case of Cassini data. An activity count occurs when the radio emission intensity is above the threshold, while an observation count occurs if the receiver is operating nominally. The observation and activity counts are sorted into 5° bins of Jovian CML and 5° bins of Io phase. Therefore, this technique leads us to compare the strong and weak emissions with the same weight.

[21] As shown in Figure 2b, the relative occurrence probability is a calculated value between 0 and 1 for each longitude and Io phase bin as the total number of activity counts divided by the total number of observation counts for each bin. Voyager data are simply recorded from a dipole antenna, whereas Cassini data are measured by a three antenna system, E_U, E_V, and E_W antennas, so the final occurrence probability of Cassini data is given by the total of the occurrence probabilities for each antenna divided by 3, the total number of antennas. This is done for each frequency. This technique is more reliable in order to avoid the null effect of any single monopoles for statistical analysis.

[22] In additional analysis for investigation of the link between Jupiter's non-Io-DAM and HOM radiation, we resort the observation and activity counts for 2° bins of Jovian CML and calculate the occurrence probability before and after the encounter of each spacecraft, but remove the data influenced by Io, which have an Io phase between 85° and 100° and between 235° and 260°.

3.2. CML Versus Io Phase

[23] An understanding of the synoptic behavior of Jupiter's radio sources is provided by a two-dimensional graph of radio emissions plotted by System III CML and Io phase. Using long-term observations made by ground stations and spacecraft, there are four significant, well-known zones where occurrence probabilities are relatively high. They are called sources D, B, A, and C, in increasing longitude sequence [*Carr et al.*, 1983]. It is known that the emission is almost elliptically or circularly polarized, in the right-hand sense for sources A and B, and in the left-hand sense for sources C and D. Since the emission is considered to be radiated in the X mode at a frequency just above the local electron gyrofrequency [see, e.g., *Kaiser and Garcia*, 1997; *Queinnec and Zarka*, 1998], sources A and B are located in the northern auroral zone and the sources C and D in the southern auroral zone.

[24] The results of the Cassini and the combined Voyager 1 and 2 analyses at 16.025 MHz and at 15.95 MHz are shown in Figures 3a and 3b plotted as a function of Jovian CML and Io phase, respectively. The enhancements in occurrence probability are seen for the Io phase near 90° and 250°. Although distinct Io-DAM components appear in each graph, the non-Io-DAM is clearly seen as the higher occurrence probability components. In particular, the Cassini occurrence probability map at 16 MHz is more likely to be that observed by ground stations at 16 MHz [see *Carr and Desch*, 1976, Figure 8; *Thieman and Smith*, 1978, Figure 7d]. On comparing the occurrence probability maps of Cassini with that of Voyager at 16 MHz, the non-Io-B region shows significantly at almost all Io phases, but different probabilities of non-Io-A and non-Io-C are exhibited in Figures 3a and 3b. This difference is because the flux densities of non-Io-A and non-Io-C observed by Voyager are weaker than that of non-Io-B [*Alexander et al.*, 1981] since the sensitivity of the Voyager/PRA receiver is about two orders of magnitude less than that of Cassini/RPWS [*Zarka and Kurth*, 2005], even though we take into account the distance correction.

[25] To investigate the dependence of the System III longitude for non-Io-DAM components, we removed the data having an Io phase between 85° and 100° and between 235° and 260°, for each frequency [*Higgins et al.*, 2006; *Higgins*, 2007; *Imai et al.*, 2008]. Figures 3c and 3d show the non-Io-related occurrence probability histograms of Cassini and of combined Voyager 1 and 2 data from 2 to 16 MHz in 2 MHz intervals in System III CML, respectively. In Figure 3c, as frequency decreases from 16 MHz down to 10 MHz, the peaks of non-Io-B and non-Io-A are shifted toward 205° CML. At 16 MHz, the peaks of non-Io-B and non-Io-A occur at 160° and 240°, but the peak eventually merges at 10 MHz near 205°. This feature called the "V-shape" was already reported by *Imai et al.* [2008]. In the case of Voyager, in Figure 3d, only the non-Io-B is shifted toward 200° from 16 MHz down to 10 MHz. The peak of non-Io-B is seen at 165° CML at 16 MHz, and at 190° CML at 10 MHz. Below 10 MHz, the Voyager occurrence probability histograms show only one region of relatively high occurrence probability, 280° ≤ CML ≤ 350° in Figure 3d, while the Cassini histograms show two broad regions, 85° ≤ CML ≤ 145° and 290° ≤ CML ≤ 5°, in Figure 3c. This is characteristic of typical HOM, having two modulations in one Jovian rotation. Comparing Cassini and Voyager, the differences can be explained by a latitudinal beaming model where the beam projects from specific magnetic latitudes [*Alexander et al.*, 1979; *Ladreiter and Leblanc*, 1989].

3.3. CML Versus Frequency

[26] To further investigate Jovian System III dependence of the Jupiter's non-Io-DAM and HOM radio emissions,

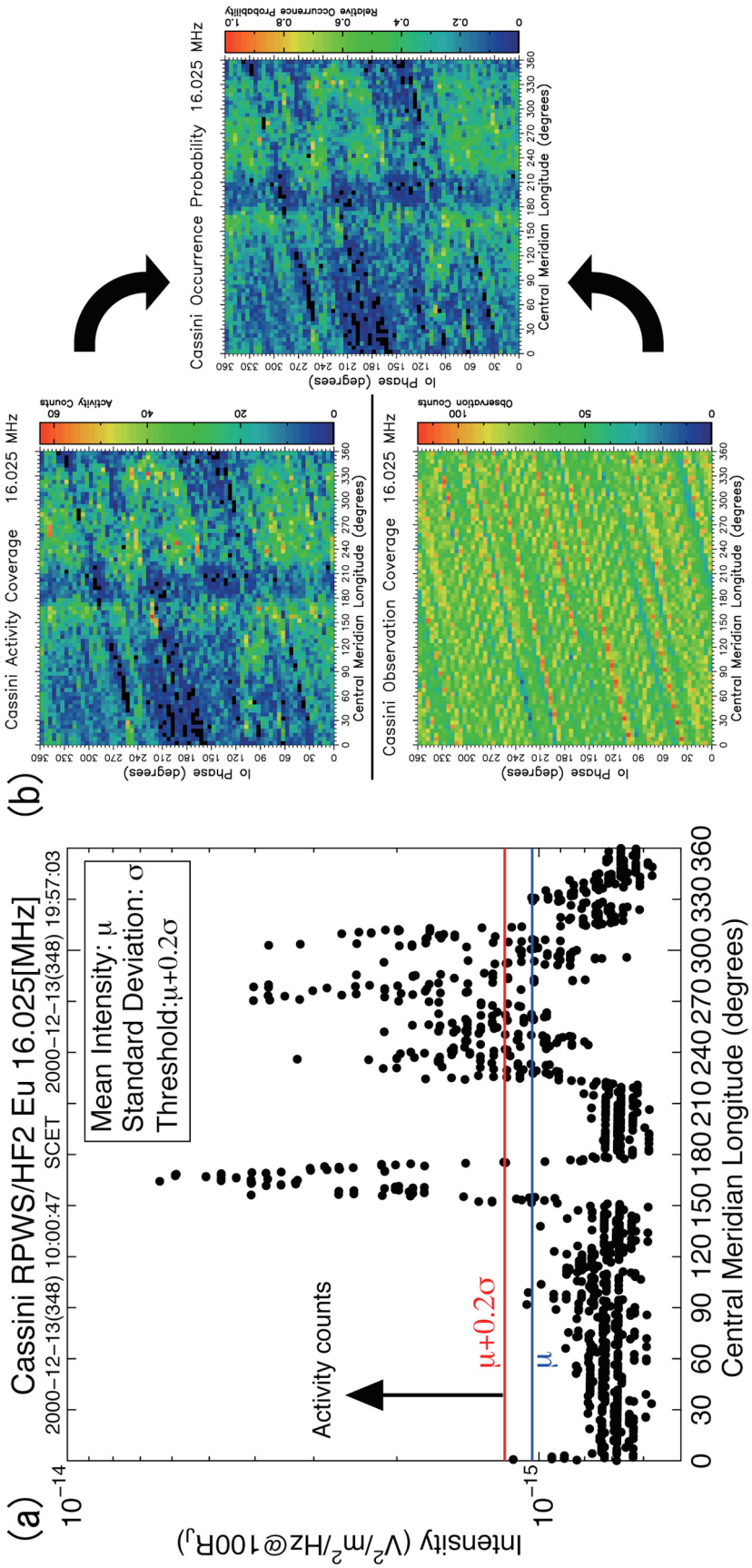

Figure 2. (a) The concept of the rotation based averaging method for Cassini data is shown. The small black dots, and the blue and the red lines indicate each calibrated spectral density, the mean intensity (μ), and the activity threshold versus CML, respectively. The activity threshold is defined as the mean intensity plus one-fifth the standard deviation (σ) of the mean ($\mu + 0.2\,\sigma$). If the radio emission intensity is above the threshold, an activity count occurs. (b) This graph shows how to deduce each bin of occurrence probability which is equal to observation counts divided by activity counts. Note that, although the graphs of occurrence probability and activity maps are similar, each unit is different.

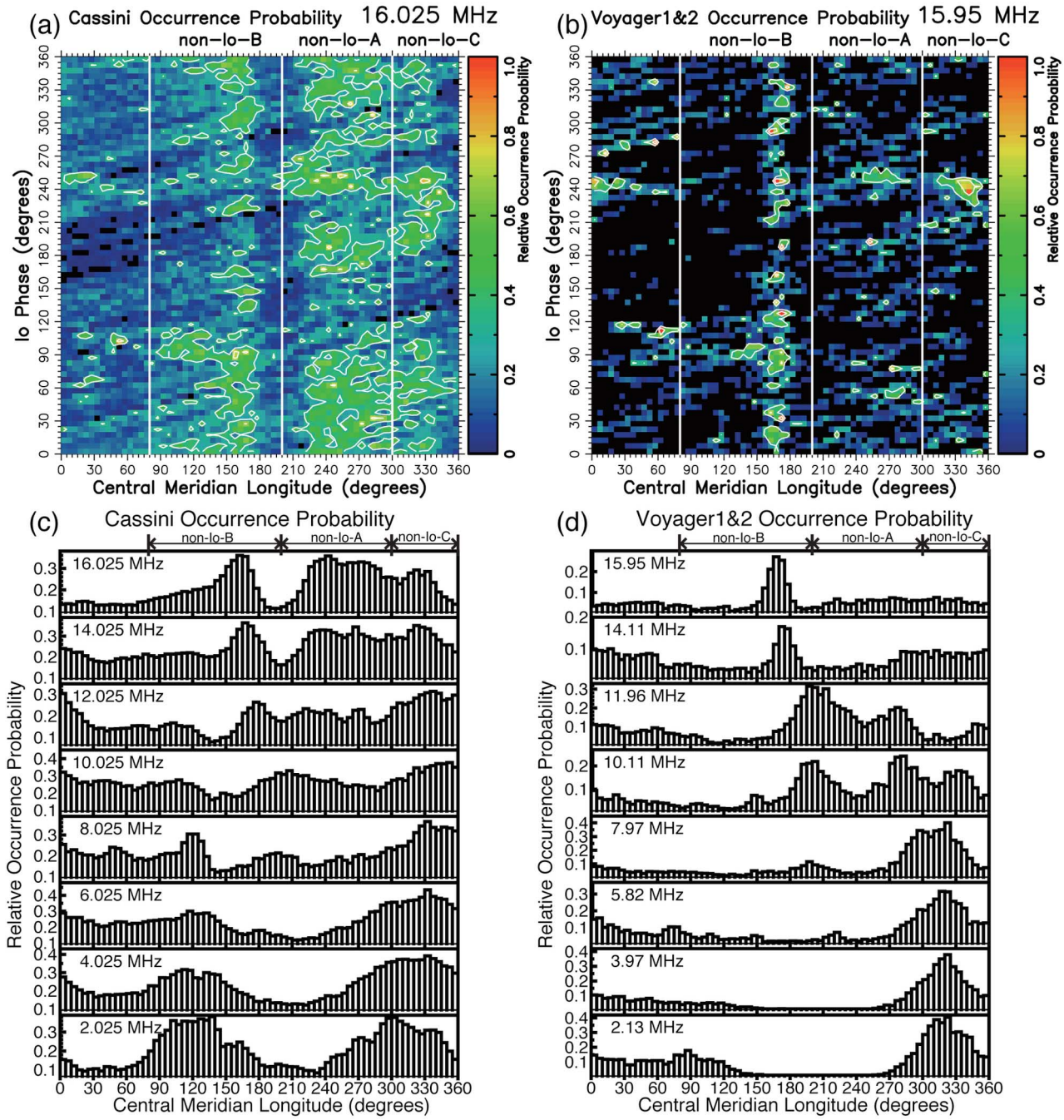

Figure 3. (a) Cassini and (b) combined Voyager 1 and 2 data at 16.025 MHz and at 15.95 MHz are shown as a probability of occurrence graph for Jovian CML versus Io phase. The occurrence probability color scale is shown at the right of each graph. The superimposed white contours are at occurrence probability of 33 and 66%. The non-Io-B region, from 80° to 200° CML, the non-Io-A, from 200° to 300° CML, and the non-Io-C, from 300° to 360° CML, are separated by vertical white lines [cf. *Carr et al.*, 1983]. Histograms of non-Io-related occurrence probability (i.e., integration of all occurrence probability except for the values of Io phase between 85° and 100° and between 235° and 260° which are the regions where there is dependence on Io) based on (c) all Cassini and (d) combined Voyager 1 and 2 data from 2 to 16 MHz in 2 MHz steps are plotted as a function of Jovian CML.

we plot in Figure 4 a summary of occurrence probability observed by Cassini, Voyager 1, and Voyager 2 pre-encounter (inbound) and post-encounter (outbound) as a function of System III and frequency. The Voyager plots show additional frequencies from 16 to 25 MHz that Cassini does not. To compare Voyager plots to the Cassini plots only the parts below the horizontal white lines for the Voyager diagrams and above the horizontal white lines in the Cassini diagrams

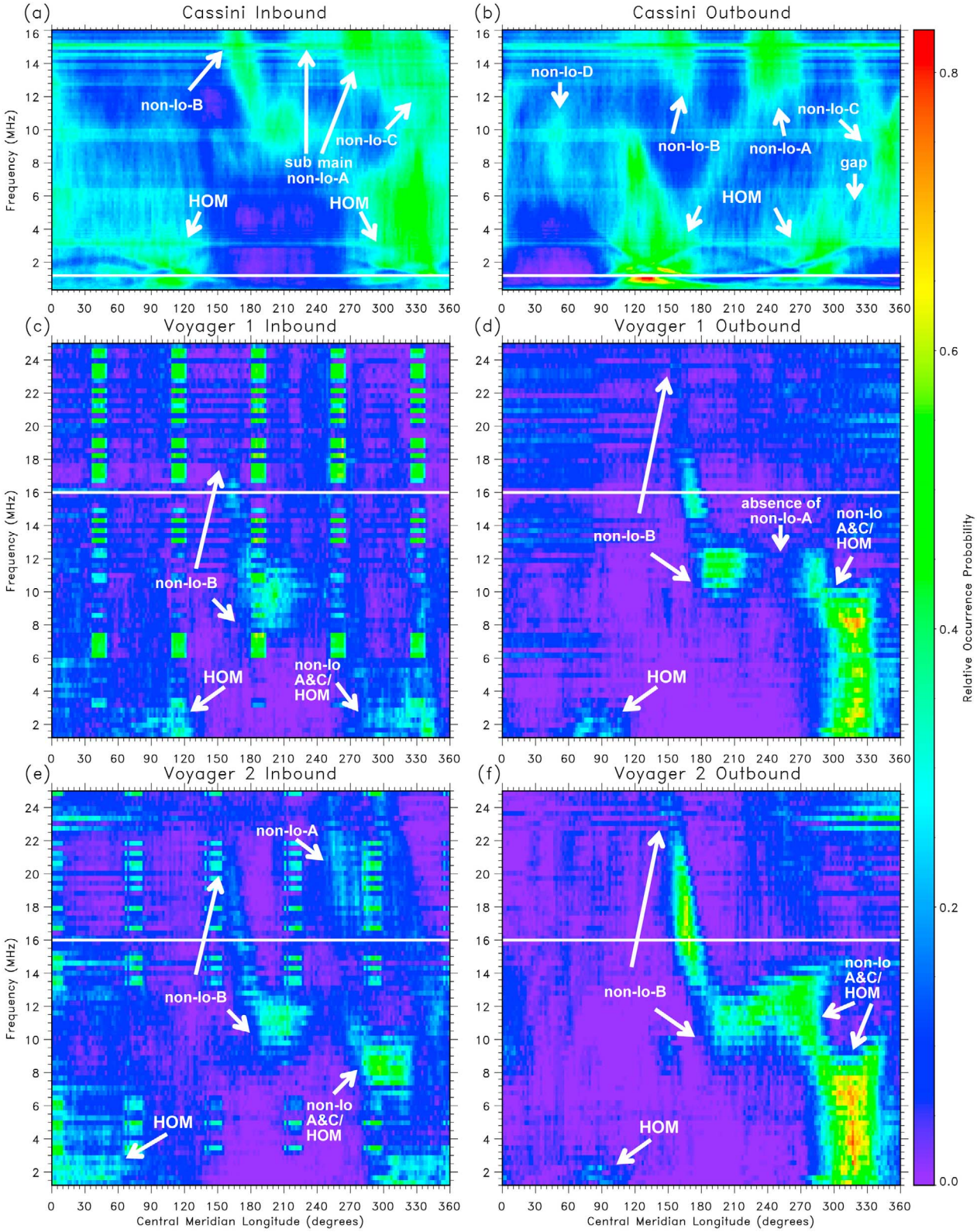

Figure 4. Occurrence probabilities of non-Io-DAM and HOM are shown as a function of Jovian System III CML. The data are taken from Cassini, Voyager 1, and Voyager 2 using (a) 187, (b) 152, (c) 64, (d) 69, (e) 74, (f) 48 planetary rotations before and after Jovian encounter. The frequency range used for Cassini and Voyager is between 0.3 MHz and 16 MHz and between 1.3 MHz and 25 MHz, respectively. The white lines indicate frequencies from 1.3 to 16 MHz that can be directly compared between Cassini and Voyager data. The occurrence probability is shown on the right side.

should be examined. The complex features can be seen in the figure, and the enhanced high probability regions are labeled non-Io-B, -A, -C, -D, and HOM, respectively. Before discussing each component, there are three main areas of interference to point out: (1) continuous interference in several frequencies of each spacecraft, especially around 15 MHz for the Cassini spacecraft, before and after encounter due to the noise coming from spacecraft itself, (2) the vertical bands of interference, like quasiperiodic noise, during Voyager 1 and Voyager 2 before encounter, because of other on-board instruments [*Alexander et al.*, 1981], and (3) the statistical noise above 22 MHz between 0° and 80° CML in Figure 4e and between 270° and 360° CML in Figure 4f during Voyager 2 before and after encounter, respectively. In short, though these regions of interference have obscured some of the natural phenomenology of Jupiter's radio emissions, the effect is minor and we are still able to investigate the complex behavior, as shown in Figure 4.

[27] In Figures 4a and 4c, we can briefly compare the sensitivity of the receivers Voyager/PRA and Cassini/RPWS, since the inbound trajectories of Voyager 1 and Cassini are similar (see Figure 1 and Table 1). These show good agreement of structure such as the distinct structure of non-Io-B and the lower part of HOM, even though the interference masks some of the real emissions. For instance, Figure 4a at 16 MHz clearly shows the enhancement of occurrence probability of non-Io-A and non-Io-C, while there is relatively little or no occurrence probability in the non-Io-A and non-Io-C regions in Figure 4c; again, the sensitivity of Cassini/RPWS is much higher than that of Voyager/PRA [*Zarka and Kurth*, 2005].

[28] It is important to note that the non-Io-B can also be seen in Plate 1 of *Alexander et al.* [1981] in both the pre- and post-encounter data from Voyager 1 as well as Voyager 2. There was no discussion of the non-Io-B feature in that paper. We find that there is a distinct structure of non-Io-B from 25 MHz down to 9 MHz in Figure 4, except for Figure 4b where it ends at 12 MHz. This non-Io-B is quasiperiodic emission and has an occurrence rate of about 0.5. Moreover, the width of non-Io-B at 25 MHz ($140° \leq$ CML $\leq 160°$) is much sharper than that at 10 MHz ($180° \leq$ CML $\leq 240°$). This agrees with *Barrow* [1981a], who found the fixed width of non-Io-B between 150° and 170° CML based on the statistical analysis of the data above 15 MHz from ground observations, Voyager 1, and Voyager 2. However, he did not point out the frequency dependence on the width, and also did not find the 9 MHz lower limit of the non-Io-B feature.

[29] On examination of non-Io-A above 16 MHz, a reasonably good example is seen in Figure 4e at frequencies from 16 to 25 MHz. The non-Io-A in Figure 4e dominates from 240° to 300° CML among Figure 4, in part because of a local time effect [*Alexander et al.*, 1981; *Leblanc*, 1981; *Barrow*, 1981a]. Despite similar trajectory parameters of Voyager 1 inbound compared with Voyager 2 inbound, there is no remarkable structure of the non-Io-A above 16 MHz in Figure 4c due in part to the higher occurrence of the vertical bands of interference than in Figure 4e. On the other hand, in Figure 4a, there are two different components of non-Io-A below 16 MHz named here as a sub component ($210° \leq$ CML $\leq 260°$) and main component ($260° \leq$ CML $\leq 310°$). The former appears to connect the edge of non-Io-B near 210° CML at 9 MHz, while the latter is more likely to extend down to 12 MHz near 270° CML. By contrast, in Figure 4b, there is one peak of non-Io-A at 16 MHz ($230° \leq$ CML $\leq 270°$). The different sizes of the width of non-Io-A are possibly explained by the changes of Jovigraphic latitude of the Cassini spacecraft during inbound and outbound passes, from 3.7° to −3.7°, respectively. These features exactly correspond to the latitudinal change of the observer, called the latitudinal effect, or declination of the earth (D_E) effect, which, in particular, has a clearer effect on the behavior of non-Io-A emission [*Carr and Desch*, 1976; *Carr et al.*, 1983; *Barrow*, 1981a; *Garcia*, 1996]. Previous studies have not discussed the frequency dependence of non-Io-A, so we report for the first time the sub and main components in the non-Io-A region.

[30] We now discuss the combined non-Io-A/C and HOM in Figure 4. The figure helps facilitate the identification of non-Io-A/C and HOM (i.e., whether or not these components are independent of each other). In Figure 4b at 5 MHz, we find a small gap between HOM and non-Io-C from 316° to 322° CML, where the minimum is seen in the occurrence probability. It implies HOM and non-Io-C emissions might come from different source regions since the occurrence probability of HOM is independent of that of non-Io-C. Hence combined non-Io-A/C and HOM is probably due to the changing observational position of each spacecraft (see Figure 1). It is important to note that there are similar plots in Figures 4d and 4f, because the passes of both Voyager 1 and 2 outbound have similar local time. There are different signatures between 220° and 270° CML from 10 to 14 MHz in Figures 4d and 4f. In Figure 4d, the part of non-Io-A is not seen, while non-Io-A seemingly connects to the edge of non-Io-B as well as of part of non-Io-C in Figure 4f. This might be due to the latitudinal directivity of the non-Io-A source. In this study, the Voyager 1 and 2 outbound data correspond to the Jovigraphic latitude range of 3.8° to 5.3° and −0.9° to 5.2°, respectively. This could be due to the dominance of the non-Io-A beam below 3.8° Jovigraphic latitude.

[31] In connection with HOM, it is obvious that two broad regions of the periodic features can be seen in Figure 4. Many studies attempted to investigate whether or not the higher part of HOM corresponds to a part of the non-Io-DAM. The higher frequency of HOM is suggested to be 3 MHz [*Carr et al.*, 1983] and 7 MHz [*Barrow and Desch*, 1989], yet it is not fully understood. One of the interesting HOM characteristics is the attenuation band, or "lane" structure, within HOM radiation [*Higgins et al.*, 1995]. This phenomenon can be explained by ray refraction from a higher plasma density along Io's L-shell [*Gurnett et al.*, 1998; *Menietti et al.*, 2003] since the source of HOM is believed to be $7 \leq L \leq 11$ [*Ladreiter et al.*, 1994] or $L \geq 10$ [*Menietti et al.*, 2003]. This obvious attenuation band can be seen in Figures 4a and 4b as well as in Figures 4c–4f as a relatively small fluctuation of occurrence probability below 2 MHz. The lower frequency receiver, which is designed to detect the frequencies from a few kHz to 1.3 MHz on-board Voyager, shows clearly this attenuation structure [see *Higgins et al.*, 1995, 1998]. By means of the higher sensitivity of Cassini/RPWS, for the first time, we can distinguish the higher part of HOM extending up to 10 MHz in Figure 4b. The other lower frequency part of HOM from 260° to 315° CML in Figure 4b appears to show the upper frequency at 6 MHz,

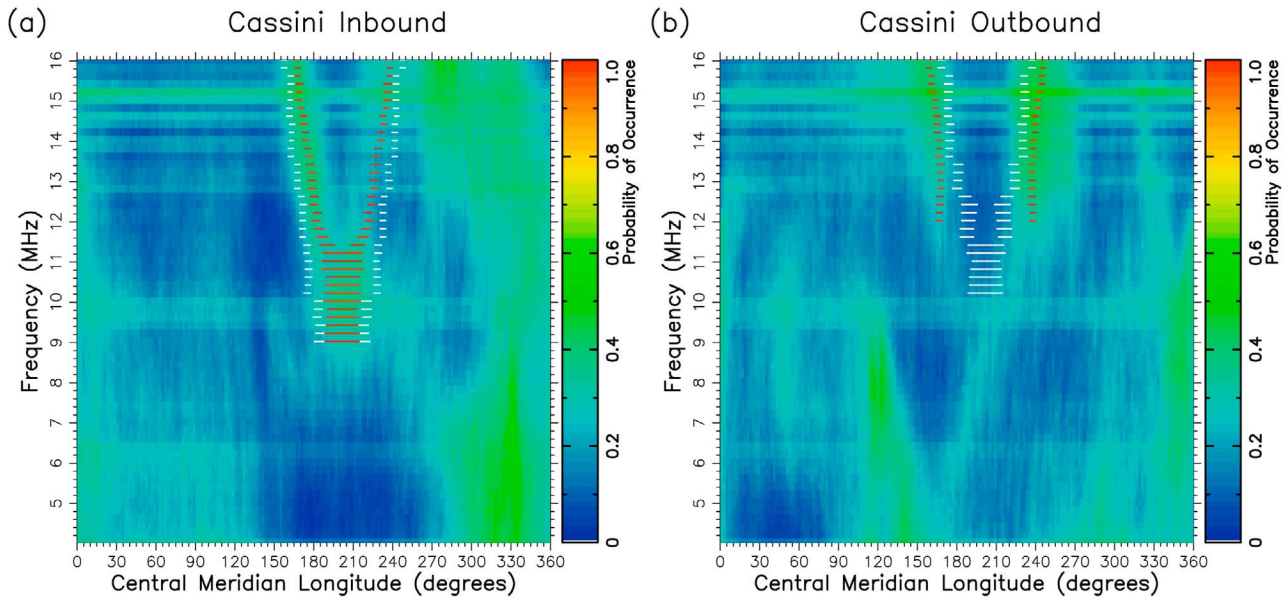

Figure 5. These graphs show the occurrence probability of (a) Cassini inbound, at 3.7°, and (b) outbound, at −3.7°, transformed from Figures 4a and 4b displaying just the frequencies from 4 to 16 MHz, as a function of Jovian System III CML. The white horizontal lines represent the calculated result from the modeled angle of *Imai et al.* [2008], and the red horizontal lines show the result from the modified angle used in this study. The occurrence probability is shown on the right side of each graph.

since the occurrence probability of HOM might decrease when the frequency increases. In Figures 4c–4f, the two peaks of HOM at lower frequency at 1.3 MHz exactly correspond to the peaks of HOM at 1.3 MHz obtained by the lower frequency band of Voyager, which is higher sensitivity than high frequency receiver used in this study [*Higgins et al.*, 1998].

[32] Finally, in Figure 4b, we found the enhancement of occurrence probability from 40° to 60° CML in the frequency range from 7 to 11 MHz is a new component, named the non-Io-D. The non-Io-D is independent of any other components; its observation on Figure 4b only is possibly either a local time effect or a latitudinal effect. This will be the subject of future study.

4. Modeling the Emission Pattern

[33] Although there is a lot of complex phenomenology in Figure 4, we focus on the non-Io-B and non-Io-A features as observed by Cassini before and after encounter. Recently, *Imai et al.* [2008] proposed an angular beaming model, based on the combined Cassini occurrence probability map, that decreases the cone half-angle of the emitting source as frequency decreases from 16 MHz down to 9 MHz. We have extended this model according to the new observations of the "V-shape" feature before and after encounter of the Cassini spacecraft. To explain these features we assume that the radio sources are located along magnetic field lines that are continuously producing DAM emission, the so-called "active magnetic flux tubes", and use straight-line propagation of radio emissions from a source region at frequencies approximately equal to the local electron cyclotron frequencies. We then determine the source locations and wave normal angle initially using the VIP4 magnetic field model [*Connerney et al.*, 1998]; results were later checked using the VIT4 magnetic field model (J. E. Connerney, personal communication, 2008). Briefly, the VIP4 model is derived from the magnetic measurement taken by Voyager and Pioneer 10 and the infra-red (IR) observations of the Io flux tube footprint, whereas the VIT4 model is determined without the Pioneer 10 observations. A detailed description of the VIT4 and the VIP4 models can be found in the work given by *Ray and Hess* [2008]. In our model we change the position of the observer (Cassini) to be at latitude = 3.7° before encounter and at latitude = −3.7° after encounter, but the observer remains at a fixed distance r = 100 R_J. In addition, the beam width is less than 2° [*Kaiser et al.*, 2000] with a fixed thin hollow cone beam.

[34] Figure 5 shows the occurrence probability calculated from the Cassini inbound and outbound data plotted as a function of frequency and CML for the frequency range of 4 to 16 MHz. The white and red horizontal lines superimposed on these graphs show the calculated results from the modeled cone half-angle at the 198° active magnetic flux tube (the projected System III longitude on Jupiter's surface is 181°) at the equator for L-shell = 5.9 by using *Imai et al.*'s [2008] and our updated models, respectively. The widths of the horizontal lines indicate the observable range at the cone half-angle of the emitting cone. In fact, the occurrence probability of Cassini inbound and outbound cannot be clearly explained by *Imai et al.* [2008], whose model is a fixed cone half-angle. Thus, we have attempted to fit the cone half-angle, shown as the red lines in Figure 5 as our updated model. The improved emitting cone with 49° half-angle at 16 MHz is seen in two sections, 167° ± 2° and 237° ± 2° in System III CML in Figure 5a for the observer at 3.7°. However, the cone with 60° half-angle is seen in two sections, 159° ± 2° and 245° ± 2° CML in Figure 5b for the observer

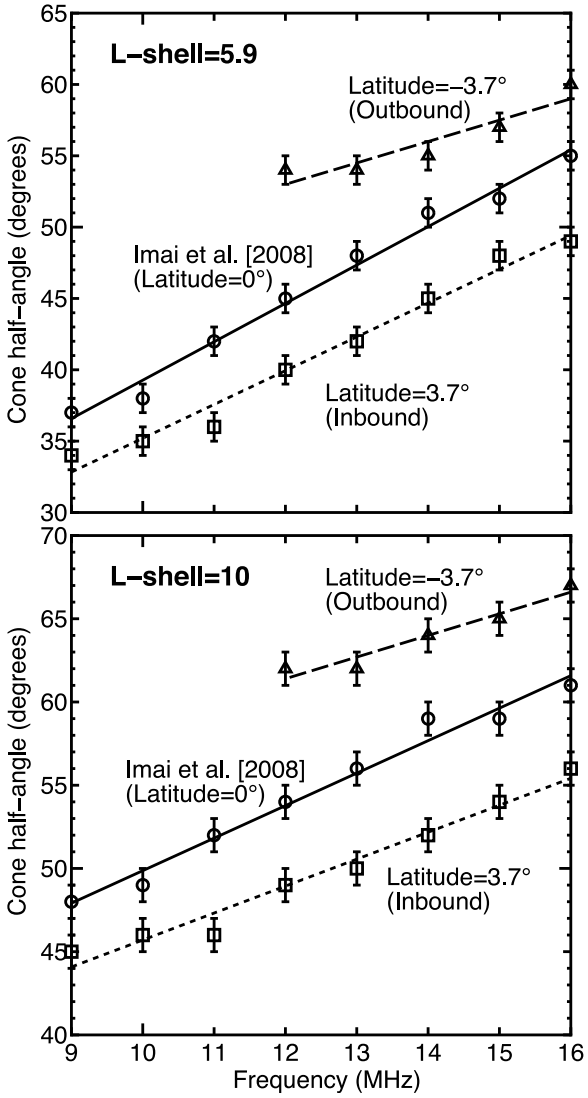

Figure 6. These graphs plot the best fitting cone half-angle of the V-shape pattern versus frequency from 9 to 16 MHz for 1 MHz intervals at L-shell = 5.9 (upper plot) and 10 (lower plot).

at −3.7°. As the frequency decreases to 9 MHz, the emitting cone with 34° cone half-angle occurs in only one section between 188° and 214° CML in Figure 5a, for the observer at 3.7°. In contrast, in Figure 5b with the observer at −3.7°, as the frequency decreases to 12 MHz, the emitting cone with 54° cone half-angle is still seen in two sections at 166° ± 2° and 237° ± 2° CML. Since the occurrence probability rapidly declines below 12 MHz, we cannot simulate the cone half-angle; it is probably due to the beaming form. This is a subject for further study.

[35] Another model, proposed by *Shaposhnikov et al.* [1997], created for the origin of the main polarization features of Jupiter's DAM emission above 10 MHz observed by Nançay Decameter Array [*Dulk et al.*, 1994] is based on moderate linear mode coupling in Jupiter's magnetosphere; they calculated the cone half-angle for sources A and B (i.e., linear polarization degree r_l 0.65 and 0.85) to be ≥63° and ≥73°, respectively. These cone half-angles are greater than our estimation; however, they are dependent on the measurements of r_l, which are not fully understood since there is a lack of Jovian DAM and HOM polarization senses in the frequency range between 1.3 MHz and 10 MHz. The polarization senses of DAM above 10 MHz and HOM below 1.3 MHz are known as elliptical [*Dulk et al.*, 1994] and pure circular [*Ortega-Molina and Lecacheux*, 1991], respectively.

[36] For a source along L-shell = 10, the values of both cone half-angles at 3.7° and −3.7° latitude are slightly different, but the feature of the cone half-angle is similar to the case for L-shell = 5.9. In Figure 6 we show the estimated cone half-angle versus frequency plots, from 9 to 16 MHz in 1 MHz steps to fit the V-shape pattern for L-shell values 5.9 and 10. Note that error bars correspond to the beaming width of less than 2° [*Kaiser et al.*, 2000]. According to the Cassini outbound, we cannot simulate the cone half-angle below 12 MHz, since the occurrence probability rapidly decreases. However, we conclude two main results: (1) the cone half-angle from 16 MHz down to 9 MHz tends to shrink depending on frequency, and (2) the cone half-angle at −3.7° is larger than that at 3.7°.

[37] Regarding the first result, this is in agreement with *Imai et al.* [2008] and *Ray and Hess* [2008], who report the cone half-angle decreases when the frequency decreases in the case of non-Io-DAM and Io-DAM, respectively. Insofar as we assume the symmetrical hollow cone model against the second result, we conclude that the changing cone half-angle is not due to a latitudinal effect. Moreover, we now believe that the second result is due to a local time effect since the Cassini inbound covers from 10.6 to 12.8 hours, while the Cassini outbound monitors 19.2 to 21.4 hours. Hence, the environment of plasma around the source region when Cassini observes the noon side tends to be a higher density profile because of the Sun, while the condition around the source when Cassini observes the night side is more likely to be a lower density profile. The angular dependence of the growth rate is very sensitive to the ratios ω_{pe}^2/Ω_e^2 and n_e/n_b [*Wong et al.*, 1982; *Wu*, 1985], where ω_{pe}^2 and Ω_e^2 are the electron plasma frequency and the electron cyclotron frequency, and n_e and n_b are the number densities of the energetic and background electrons. Thus, the growth rates vary with wave normal angle [*Wong et al.*, 1982; *Wu*, 1985]. In conclusion, we cannot explain the different cone half-angles based on a latitudinal effect, rather we believe the changing cone half-angle is due to the local time effect.

[38] On the basis of the peak width of the non-Io-B source between 148° and 182° CML and between 140° and 170° CML at 16.025 MHz during inbound and outbound of Cassini, we have investigated the source locations using our model. In Table 2, we list the calculated L-shell values, the position of observer's latitude, the corresponding range of System III longitudes of the intersection of the active magnetic flux tubes with the equatorial plane, and the range of the projected longitudes on Jupiter's surface. Both non-Io-B and non-Io-A sources are localized at about 180° ± 10° (at L-shell = 5.9), or about 180° ± 5° (at L-shell = 10), of System III longitude projected on Jupiter's surface.

[39] We repeated our calculations using the VIT4 magnetic field model instead of the VIP4 model. The resulting differences were very small, in no way affecting our conclusions.

Table 2. Locations of the Non-Io-A and Non-Io-B Sources at Different Latitudes of Observer for L-shell = 5.9 and 10

L-shell	Latitude of Observer[a]	Active Magnetic Flux Tubes[b]	Projected System III Longitude on Jupiter's Surface
5.9	3.7°	190°–220°	178°–193°
5.9	−3.7°	170°–195°	169°–180°
10	3.7°	175°–210°	171°–185°
10	−3.7°	180°–205°	173°–183°

[a]The positions of Cassini inbound and outbound corresponding to an observer's latitude of 3.7° and −3.7° respectively.

[b]The corresponding range of System III longitudes of the intersection of the active magnetic flux tubes with the equatorial plane.

[40] It is widely believed that non-Io-DAM is auroral radio emission from the Jovian aurora. *Prangé et al.* [1993] state that one of the characteristics of an intense auroral event in December 1990 was a shift in longitude from the statistical average value of near 180° to greater longitudes by about 60°. Moreover, the complex structures of the Jovian UV aurora have been obtained by the Hubble Space Telescope [*Clarke et al.*, 2004]. *Waite et al.* [2001] found that a strong intensity flare appeared near 167° System III longitude. During the Cassini campaign, a polar flare also occurred on 14 December 2000 around 170° System III longitude [*Grodent et al.*, 2003]. Our results of 180° ± 10° are close to the values of longitudes of these UV auroral phenomena. The relationship between UV aurora and non-Io-DAM emission gives further weight to our model.

5. Conclusions

[41] In this paper, we report the characteristics of Jupiter's decameter and hectometer wavelength emissions at the frequency range from 0.3 to 25 MHz observed by the Cassini, Voyager 1, and Voyager 2 spacecraft. Despite the fact that there is some interference at the frequencies below 15 MHz recorded by Voyager 1 and Voyager 2, we have investigated the complex behaviors of Jovian DAM and HOM emissions by using the technique of producing occurrence probability graphs. Characteristics of the occurrence probability graphs lead us to reveal a new classification of Jupiter's DAM and HOM radio emissions. The main results are as follows:

[42] 1. The detailed frequency structures of non-Io-DAM and HOM are presented for different spacecraft's local time and Jovigraphic latitude. At a frequency range below 16 MHz, the non-Io-A has been classified as a sub component (210° ≤ CML ≤ 260°) and main component (260° ≤ CML ≤ 310°); the former appears to connect the edge of non-Io-B, whereas the latter seems to be independent of any other components.

[43] 2. The higher frequency of HOM extends up to 10 MHz using Cassini post-encounter data. In addition, there is a small occurrence probability gap between HOM and non-Io-C, so HOM and non-Io-C emissions might come from different source regions since the occurrence probability of HOM is independent of that of non-Io-C.

[44] 3. The Cassini outbound occurrence probability plot indicates a new DAM component called the non-Io-D source region is located from 40° to 60° CML in the frequency range of 7–11 MHz.

[45] 4. The local time of an observation is critical; our model requires a different size emission cone for different local times. For instance, the emission cone half-angle at 16 MHz is measured to be 49° for local times near 11 hours and 60° for local times near 20 hours.

[46] **Acknowledgments.** The authors are pleased to acknowledge the Cassini RPWS team for access to the Cassini data at the Planetary Data System (PDS) and J. Groene (University of Iowa) for creating Cassini and Voyager ephemeris tables. The authors are especially grateful to J.E.P. Connerney for providing the VIT4 magnetic field model and A. Lecacheux and P. Zarka for numerous discussions. M.I. would like to acknowledge support from M. Fujimoto (JAXA) during a four-month visit to the Observatoire de Paris-Meudon. This work was supported by the Ministry of Education, Culture, Sports, Science and Technology, Grant-in-Aid for Scientific Research (B), 19340142.

[47] Masaki Fujimoto would like to thank the reviewers for their assistance in evaluating this paper.

References

Alexander, J. K., M. D. Desch, M. L. Kaiser, and J. R. Thieman (1979), Latitudinal beaming of Jupiter's low frequency radio emissions, *J. Geophys. Res.*, *84*, 5167–5174.

Alexander, J. K., T. D. Carr, J. R. Thieman, J. J. Schauble, and A. C. Riddle (1981), Synoptic observations of Jupiter's radio emissions: Average statistical properties observed by Voyager, *J. Geophys. Res.*, *86*, 8529–8545.

Aubier, M. G., and F. Genova (1985), A catalogue of the high frequency limit of the Jovian decameter emission observed by Voyager, *Astron. Astrophys. Suppl. Ser.*, *61*, 341–351.

Barrow, C. H. (1981a), Latitudinal beaming and local time effects in the decametre-wave radiation from Jupiter observed at the Earth and from Voyager, *Astron. Astrophys.*, *101*, 142–149.

Barrow, C. H. (1981b), A catalogue of Jupiter's decametric emission observed by Voyager-1 and by Voyager-2 in the range 15–40 MHz, *Astron. Astrophys. Suppl. Ser.*, *46*, 111–114.

Barrow, C. H., and M. D. Desch (1989), Solar wind control of Jupiter's hectometric radio emission, *Astron. Astrophys.*, *213*, 495–501.

Bigg, E. K. (1964), Influence of the satellite Io on Jupiter's decametric emission, *Nature*, *203*, 1008–1010.

Boischot, A., et al. (1980), A new high-gain, broadband, steerable array to study Jovian decametric emission, *Icarus*, *43*, 399–407.

Boischot, A., A. Lecacheux, M. L. Kaiser, M. D. Desch, J. K. Alexander, and J. W. Warwick (1981), Radio Jupiter after Voyager: An overview of the planetary radio observations, *J. Geophys. Res.*, *86*, 8213–8226.

Bougeret, J.-L., et al. (1995), WAVES: The radio and plasma wave investigation on the WIND spacecraft, *Space Sci. Rev.*, *71*, 231–263.

Brown L. W. (1974), Spectral behavior of Jupiter near 1 MHz, *Astrophys. J.*, *194*, L159–L162.

Carr, T. D., and M. D. Desch (1976), Recent decametric and hectometric observations of Jupiter, in *Jupiter*, edited by T. Gehrels, pp. 693–737, Univ. of Ariz. Press, Tucson.

Carr, T. D., A. G. Smith, H. Bollhagen, J. N. F. Six, and N. E. Chatterton (1961), Recent decameter-wave-length observations of Jupiter, Saturn, and Venus, *Astrophys. J.* , *134*, 105–125.

Carr, T. D., M. D. Desch, and J. K. Alexander (1983), Phenomenology of magnetospheric radio emissions, in *Physics of the Jovian Magnetosphere*, edited by A. J. Dessler, pp. 226–284, Cambridge Univ. Press, New York.

Clarke, J. T., D. Grodent, S. W. H. Cowley, E. J. Bunce, P. Zarka, J. E. P. Connerney, and T. Satoh (2004), Jupiter's aurora, in *Jupiter: The Planet, Satellites and Magnetosphere*, edited by F. Bagenal, T. E. Dowling, and W. B. McKinnon, pp. 639–670, Cambridge Univ. Press, New York.

Connerney, J. E. P., M. H. Acuña, N. F. Ness, and T. Satoh (1998), New models of Jupiter's magnetic field constrained by the Io flux tube footprint, *J. Geophys. Res.*, *103*, 11,929–11,939.

Desch, M. D., and T. D. Carr (1974), Dekametric and hectometric observations of Jupiter from the RAE-1 satellite, *Astrophys. J.*, *194*, L57–L59.

Dulk, G. A., Y. Leblanc, and A. Lecacheux (1994), The complete polarization state of Io-related radio storms from Jupiter: A statistical study, *Astron. Astrophys.*, *286*, 683–700.

Garcia, L. N. (1996), Long-term periodicities in the Jovian decametric emission, Ph.D. dissertation, Univ. of Fla., Gainesville.

Genova, F., P. Zarka, and C. H. Barrow (1987), Voyager and Nançay observations of the Jovian radio-emission at different frequencies: Solar wind effect and source extent, *Astron. Astrophys.*, *182*, 159–162.

Grodent, D., J. T. Clarke, J. H. Waite Jr., S. W. H. Cowley, J.-C. Gérard, and J. Kim (2003), Jupiter's polar auroral emissions, *J. Geophys. Res.*, *108*(A10), 1366, doi:10.1029/2003JA010017.

Gurnett, D. A., W. S. Kurth, J. D. Menietti, and A. M. Persoon (1998), An unusual rotationally modulated attenuation band in the Jovian hectometric radio emission spectrum, *Geophys. Res. Lett.*, *25*, 1841–1844.

Gurnett, D. A., et al. (2002), Control of Jupiter's radio emission and aurorae by the solar wind, *Nature*, *415*, 985–987.
Gurnett, D. A., et al. (2004), The Cassini radio and plasma wave investigation, *Space Sci. Rev.*, *114*, 395–463.
Higgins, C. A. (2007), Satellite control of Jovian 2–6 MHz radio emission using Voyager data, *J. Geophys. Res.*, *112*, A05213, doi:10.1029/2006JA012100.
Higgins, C. A., J. L. Green, J. R. Thieman, S. F. Fung, and R. M. Candey (1995), Structure within Jovian hectometric radiation, *J. Geophys. Res.*, *100*, 19,487–19,496.
Higgins, C. A., T. D. Carr, and F. Reyes (1996), A new determination of Jupiter's radio rotation period, *Geophys. Res. Lett.*, *23*, 19, 2653–2656.
Higgins, C. A., J. R. Thieman, S. F. Fung, J. L. Green, and R. M. Candey (1998), Latitudinal structure within Jovian hectometric radiation, *J. Geophys. Res.*, *103*, 26,679–26,686.
Higgins, C. A., J. D. Menietti, and I. W. Christopher (2006), Europa control of Jovian radio emission: A Galileo study, *Geophys. Res. Lett.*, *33*, L14110, doi:10.1029/2006GL026218.
Imai, K., L. Wang, and T. D. Carr (1997), Modeling Jupiter's decametric modulation lanes, *J. Geophys. Res.*, *102*, 7127–7136.
Imai, K., J. J. Riihimaa, F. Reyes, and T. D. Carr (2002), Measurement of Jupiter's decametric radio source parameters by the modulation lane method, *J. Geophys. Res.*, *107*(A6), 1081, doi:10.1029/2001JA007555.
Imai, M., K. Imai, C. A. Higgins, and J. R. Thieman (2008), Angular beaming model of Jupiter's decametric radio emissions based on Cassini RPWS data analysis, *Geophys. Res. Lett.*, *35*, L17103, doi:10.1029/2008GL034987.
Kaiser, M. L., and L. N. Garcia (1997), Jupiter's low-frequency radio spectrum: Filling in the gaps, in *Planetary Radio Emissions IV*, edited by H. O. Rucker, S. J. Bauer, and A. Lecacheux, pp. 17–24, Austrian Acad. Sci. Press, Vienna.
Kaiser, M. L., P. Zarka, W. S. Kurth, G. B. Hospodarsky, and D. A. Gurnett (2000), Cassini and Wind stereoscopic observations of Jovian nonthermal radio emissions: Measurement of beam widths, *J. Geophys. Res.*, *105*, 16,053–16,062.
Ladreiter, H. P., and Y. Leblanc (1989), Jovian hectometric radiation: Beaming, source extension, and solar wind control, *Astron. Astrophys.*, *226*, 297–310.
Ladreiter, H. P., and Y. Leblanc (1991), The Jovian hectometric radiation: An overview after the Voyager mission, *Ann. Geophys.*, *9*, 784–796.
Ladreiter, H. P., P. Zarka, and A. Lecacheux (1994), Direction finding study of Jovian hectometric and broadband kilometric radio emissions: Evidence for their auroral origin, *Planet. Space Sci.*, *42*, 913–931.
Lang, G. J., and R. G. Peltzer (1977), Planetary Radio Astronomy Receiver, *IEEE Trans.*, *13*, 466–472.
Leblanc, Y. (1981), On the arc structure of the DAM Jupiter emission, *J. Geophys. Res.*, *86*, 8546–8560.
Lecacheux, A. (2000), The Nançay Decameter Array: A useful step towards giant, new generation radio telescopes for long wavelength radio astronomy, in *Radio Astronomy at Long Wavelengths*, *Geophys. Monogr. Ser.*, vol. 119, edited by R. G. Stone et al., pp. 321–328, AGU, Washington, D. C.
Menietti, J. D., D. A. Gurnett, W. S. Kurth, and J. B. Groene (1999), Local time dependence of Jovian radio emissions observed by Galileo, *Geophys. Res. Lett.*, *26*, 569–572.
Menietti, J. D., D. A. Gurnett, G. B. Hospodarsky, C. A. Higgins, W. S. Kurth, and P. Zarka (2003), Modeling radio emission attenuation lanes observed by the Galileo and Cassini spacecraft, *Planet. Space Sci.*, *51*, 533–540.
Ortega-Molina, A., and A. Lecacheux (1991), Polarization of Jovian hectometric emission, *J. Geophys. Res.*, *96*, 11,441–11,453.
Prangé, R., P. Zarka, G. E. Ballester, T. A. Livengood, L. Denis, T. Carr, F. Reyes, S. J. Bame, and H. W. Moos (1993), Correlated variations of UV and radio emissions during an outstanding Jovian auroral event, *J. Geophys. Res.*, *98*, 18,779–18,791.
Queinnec, J., and P. Zarka (1998), Io–controlled decameter arcs and Io–Jupiter interaction, *J. Geophys. Res.*, *103*, 26,649–26,666.
Ray, L. C., and S. Hess (2008), Modelling the Io-related DAM emission by modifying the beaming angle, *J. Geophys. Res.*, *113*, A11218, doi:10.1029/2008JA013669.
Shaposhnikov, V. E., V. V. Kocharovsky, V. V. Kocharovsky, H. P. Ladreiter, H. O. Rucker, and V. V. Zaitsev (1997), On elliptical polarization of the decametric radio emission and the linear mode coupling in the Jovian magnetosphere, *Astron. Astrophys.*, *326*, 386–395.
Terasawa, T., K. Maezawa, and S. Machida (1978), Solar wind effect on Jupiter's non-Io-related radio emission, *Nature*, *273*, 131–132.
Thieman, J. R., and A. G. Smith (1978), Frequency and time dependence of the Jovian decametric radio emissions: A nineteen-year high-resolution study, *J. Geophys. Res.*, *83*, 3303–3309.
Waite, J. H., Jr., et al. (2001), An auroral flare at Jupiter, *Nature*, *410*, 787–789.
Warwick, J. W., J. B. Pearce, R. G. Peltzer, and A. C. Riddle (1977), Planetary radio astronomy experiment for Voyager missions, *Space Sci. Rev.*, *21*, 309–327.
Warwick, J. W., et al. (1979a), Voyager 1 planetary radio astronomy observations near Jupiter, *Science*, *204*, 995–998.
Warwick, J. W., et al. (1979b), Planetary radio astronomy observations from Voyager 2 near Jupiter, *Science*, *206*, 991–995.
Wong, H. K., C. S. Wu, F. J. Ke, R. S. Schneider, and L. F. Ziebell (1982), Electromagnetic cyclotron-loss-cone instability associated with weakly relativistic electrons, *J. Plasma Phys.*, *28*, 503–525.
Wu, C. S. (1985), Kinetic cyclotron and synchrotron maser instabilities: Radio emission processes by direct amplification of radiation, *Space Sci. Rev.*, *41*, 215–298.
Wu, C. S., and L. C. Lee (1979), A theory of the terrestrial kilometric radiation, *Astrophys. J.*, *230*, 621–626.
Zarka, P. (1998), Auroral radio emissions at the outer planets: Observations and theories, *J. Geophys. Res.*, *103*, 20,159–20,194.
Zarka, P., and W. S. Kurth (2005), Radio wave emission from the outer planets before Cassini, *Space Sci. Rev.*, *116*, 371–397, doi:10.1007/s11214-005-1962-2.
Zarka, P., J. Queinnec, and F. J. Crary (2001), Low-frequency limit of Jovian radio emissions and implications on source locations and Io plasma wake, *Planet. Space Sci.*, *49*, 1137–1149.
Zarka, P., B. Cecconi, and W. S. Kurth (2004), Jupiter's low-frequency radio spectrum from Cassini/Radio and Plasma Wave Science (RPWS) absolute flux density measurements, *J. Geophys. Res.*, *109*, A09S15, doi:10.1029/2003JA010260.

C. A. Higgins, Department of Physics and Astronomy, Middle Tennessee State University, Murfreesboro, TN 37132, USA. (chiggins@mtsu.edu)
K. Imai, Department of Electrical Engineering and Information Science, Kochi National College of Technology, Monobe, Nankoku, Kochi 783-8508, Japan. (imai@ee.kochi-ct.ac.jp)
M. Imai, Department of Geophysics, Kyoto University, Kitashirakawa Oiwake-cho, Sakyo-ku, Kyoto 606-8502, Japan. (masafumi@jupiter.jp)
J. R. Thieman, Solar System Exploration Division, NASA Goddard Space Flight Center, Code 690.1, Greenbelt, MD 20771, USA. (james.r.thieman@nasa.gov)